Design and Performance of a Lead Fluoride Detector as a Luminosity Monitor

R. Pérez Benito[a], D. Khaneft[a], C. O'Connor[b,*], L. Capozza[a], J. Diefenbach[c,1], B.Gläser[a], Y. Ma[a,2], F.E. Maas[a], D. Rodríguez Piñeiro[a]

[a] *Johannes Gutenberg-Universität, Mainz, Germany*
[b] *Massachusetts Institute of Technology, Cambridge, MA, USA*
[c] *Hampton University, Hampton, VA, USA*

Abstract

Precise luminosity measurements for the OLYMPUS two-photon exchange experiment at DESY were performed by counting scattering events with alternating beams of electrons and positrons incident on atomic electrons in a gaseous hydrogen target. Final products of Møller, Bhabha, and pair annihilation interactions were observed using a pair of lead fluoride (PbF_2) Cherenkov calorimeters with custom housings and electronics, adapted from a system used by the A4 parity violation experiment at MAMI. This paper describes the design, calibration, and operation of these detectors. An explanation of the Monte Carlo methods used to simulate the physical processes involved both at the scattering vertices and in the detector apparatus is also included.

Keywords: OLYMPUS, Lead Fluoride, Møller Scattering, Bhabha Scattering

1. Introduction

1.1. Purpose

A significant discrepancy persists between the results of two classes of experiments that have measured the ratio of proton form factors, G_E/G_M [1]. The gap between data from polarization-transfer experiments and those from analyses using Rosenbluth separation could be due in part to contributions from two-photon exchange. Observable effects of this proposed explanation have been modeled in various ways [2] and a precise measurement is needed to select among the published theories. The OLYMPUS experiment [3] aims to quantify two-photon exchange over a range of four-momentum transfer of $0.4\ \mathrm{GeV}^2/c^2 < Q^2 < 2.2\ \mathrm{GeV}^2/c^2$ through a measurement of the ratio of electron-proton to positron-proton elastic scattering cross sections with a total uncertainty of less then 1%.

Installed at the DORIS storage ring at DESY, OLYMPUS collected data with a circulated 2.01 GeV lepton beam (alternating about daily between electrons and positrons) incident on a gaseous hydrogen target. Kinematics were over-constrained by coincident detection of the scattered lepton and the recoiling proton in a large-acceptance spectrometer inheriting from that used in the BLAST experiment at MIT-Bates [4]. Crucial to achieving the desired accuracy of the results is a precise measurement of the luminosity. While precision on an absolute scale is always desirable, for a result that relies on a ratio it is the precision of the relative luminosity measurement throughout the data-taking period that is of prime concern.

To this end, multiple subsystems were used to make complementary luminosity determinations based on distinct physical signals. First, slow control software provided a quick estimate based on the temperature of the target cell, the flow rate of hydrogen into the cell, and the beam current. Second, small-acceptance tracking detectors at polar scattering angles of about 12° were used to count events in that region, where the lepton-proton elastic scattering cross-section is higher than in the

* Corresponding Author
Email address: colton@mit.edu (C. O'Connor)
1 Currently with Johannes Gutenberg-Universität, Mainz, Germany
2 Currently with Advanced Meson Laboratory, Nishina Centre, RIKEN, Japan

spectrometer and where two-photon exchange effects are believed by some to be negligible. Finally, interactions between the beam and atomic electrons in the target were monitored with a pair of Cherenkov calorimeters placed about 3 m downstream of the target center at the symmetric Møller scattering angle, that is, the polar scattering angle in the lab frame common to both outgoing electrons when they have the same energy. For a beam energy of 2 GeV incident on a stationary target, this is 1.29°.

This paper describes the design and operation of these "Symmetric Møller/Bhabha" (SYMB) calorimeters. They were built to handle an accepted rate of $e^{\pm}$–e^{-} interactions (with products detected in coincidence) of typically 5 kHz. As such, the associated electronics were required to function continuously with effectively no dead time. The choice of detector material needed to be sufficiently radiation hard to maintain consistent performance levels while absorbing a significant dose of high-energy particles, while also providing a fast physical response allowing for signal collection at a kilohertz rate. These considerations lead to the use of PbF_2 crystals, in which energetic charged particles produce Cherenkov light with no scintillation component. Photomultiplier tubes gathered the light from each detector. Their output was passed through analog-to-digital converters and recorded on 8-bit by 8-bit two-dimensional histogramming cards.

1.2. Theoretical considerations

Three elastic processes contributed to the observed physical signal: Møller scattering ($e^-e^- \rightarrow e^-e^-$), Bhabha scattering ($e^+e^- \rightarrow e^+e^-$), and pair annihilation ($e^+e^- \rightarrow \gamma\gamma$). All three are pure quantum electrodynamic processes whose cross sections can be exactly calculated. Next-to-leading order corrections [5], including corrections due to radiative final states, were accounted for in the analysis by means of Monte Carlo simulation. The simple nature of these quantum interactions, along with the high acceptance-integrated cross-sections relative to those of elastic $e^{\pm}$–p scattering, provided an opportunity for very precise luminosity measurements at OLYMPUS.

2. Design

Two identical SYMB detectors were built in Mainz, one for each "sector" of OLYMPUS (the left and right sides, from the beam's perspective). Each detector consisted of a 3×3 array of lead fluoride (PbF_2) crystals placed inside a mu-metal box along with a photomultiplier tube (PMT) for each crystal and voltage dividers. Just outside the box, on the side facing the target, a lead collimator was installed. All components were fastened to a support table that allowed them to be moved away from the beam line in a controlled way in order to avoid radiation damage during DORIS injections. They could then be precisely returned back to their original positions. Fig. 1 shows the final accommodation of the SYMB detectors in the OLYMPUS apparatus, with each collimator's aperture centered at 1.29° to the beam line about 3 m from the target center.

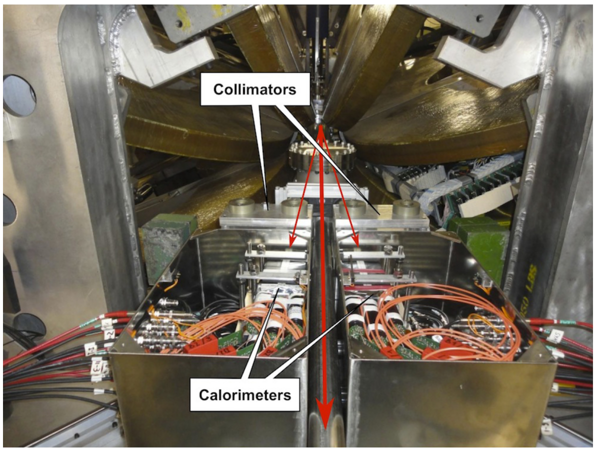

Fig. 1: Symmetric Møller/Bhabha luminosity monitors at OLYMPUS. Large red arrow indicates the beam direction; small red arrows indicate typical paths of SYMB interaction products.

2.1. Lead fluoride crystals

All crystals used in the detectors were provided by the A4 collaboration at MAMI in Mainz [6]. The lengths of the crystals, shown in Fig. 2, varied from 150.0 mm to 185.4 mm, each tapered slightly from its front (upstream) face to its back (downstream) face. These faces were trapezoids, with an area of $\sim$ 670 mm^2 for the front and $\sim$ 900 mm^2 for the back. Given lead fluoride's radiation length of 9.34 mm and Molière radius of 21.24 mm [7], such dimensions are sufficient for a 3×3 array to contain more than 95% of the energy of an electromagnetic cascade [8].

OLYMPUS was designed with an integrated luminosity goal of 4 fb^{-1}. Integrating over the region allowed by the collimator aperture, the accepted

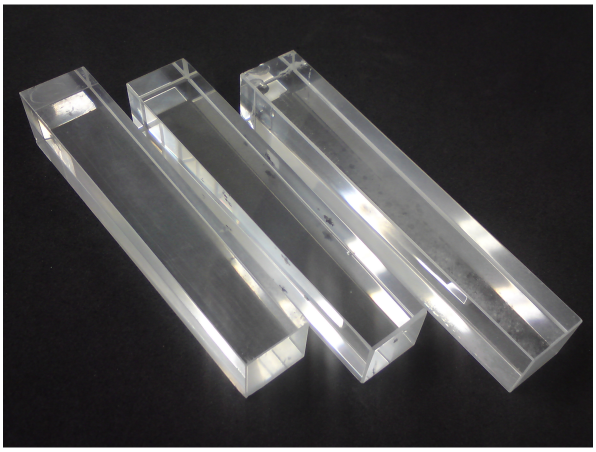

Fig. 2: PbF_2 crystals before detector assembly.

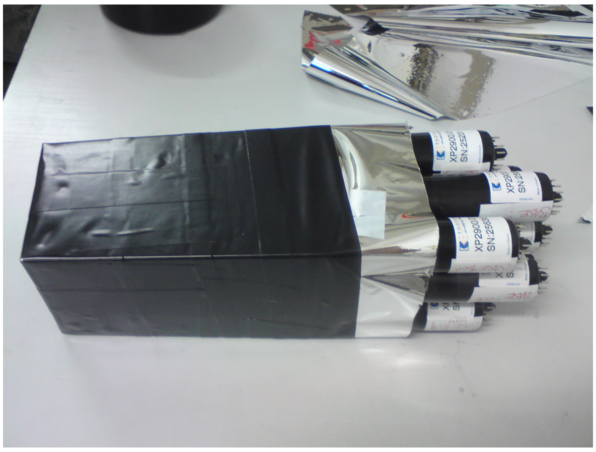

Fig. 3: Fully assembled crystal array with PMTs.

cross section was expected to be less than 50 nb for each SYMB process. With less than 1 GeV deposited in each central crystal per event, and given the size and density of the crystals, the total absorbed dose due to signal events over the course of the experiment was estimated to be no greater than 25 Gy. Allowing for some additional ionizing radiation from other sources, this was still considered safe, as even 100 Gy would be likely to cause only minor damage to the transmittance of the crystals [9].

Since lead fluoride is a pure Cherenkov material with no slow component in its light output, it has a fast response time of $\sim$5 ns. Each crystal was wrapped with Millipore paper (Immobilon-P) to improve internal reflection at the faces, then glued to a PMT (Philips XP2900/01). The custom-made PMT bases were actively stabilized to handle particle rates up to several MHz without any change in gain [10]. The completed arrays were tightly bound together by foil and tape (Fig. 3).

2.2. Collimator

Beam halo and bremsstrahlung prompted the use a lead brick collimator shielding the front of each detector. The collimator's dimensions, 200 mm$\times$100 mm$\times$120 mm, were optimized using Monte Carlo simulation studies of the bremsstrahlung background from the beam pipe.

A cylindrical aperture through the brick, 20.5 mm in diameter, was aligned to be coaxial with the long axis of the central crystal in the array. The thickness of 100 mm was sufficient to absorb all the energy of a 1 GeV lepton or photon incident on the face of the brick, except when the subsequent shower produced secondaries that escaped through the interior face of the collimator aperture. (Events of the latter kind were counted as part of our signal if they passed energy distribution cuts; see Sec. 4.) Collimators were constructed out of two pieces: the main bulk of the brick, and a small insert piece consisting of the aperture and a small region of lead surrounding it. This approach was chosen so that the dimensions of the aperture could be decreased by using a different insert if the background rate was found to be too high.

Fig. 4: Collimators *in situ*. Photo taken during final alignment, some survey equipment pictured atop collimators.

2.3. Mu-metal box and driving unit

OLYMPUS used eight copper coils to generate a toroidal field of about 0.28 T in the region of the

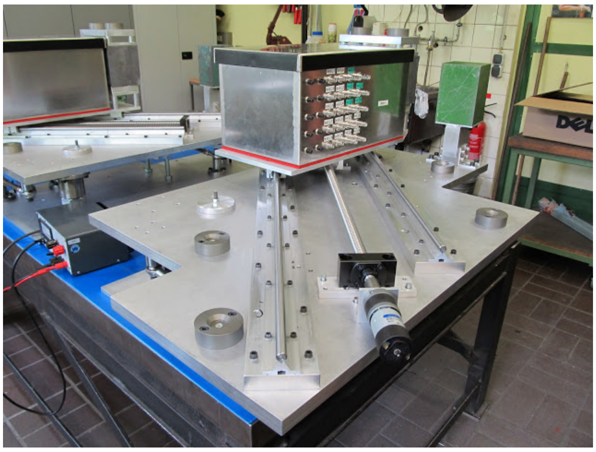

Fig. 5: SYMB table, rails, and driving unit during assembly at the mechanical workshop at Mainz University (IKPH).

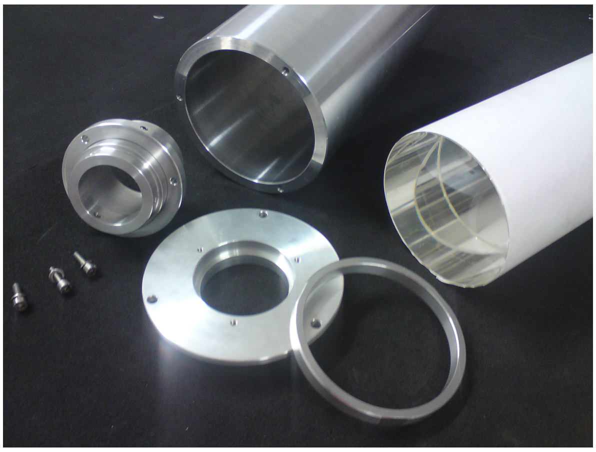

Fig. 6: Light source and cylindrical plastic diffusor tested at Mainz University (IKPH).

tracking detectors. As a result, a non-uniform field on the order of 10^{-3} T existed in the region SYMB products passed through to reach the calorimeters.

Due to the limited space available at the desired position relative to the target, shielding the crystals and PMTs from the magnetic field was a challenge. The solution was to house each crystal array, along with associated PMTs and voltage dividers, within a mu-metal box. Simulations demonstrated that a thickness of 3 mm provided sufficient shielding.

The SYMB apparatus tables featured an accurate, remotely driven rail system that allowed the boxes to move between "measurement position" at 1.29° from the beam axis and "parking position" further away from the beam pipe. Extra lead shielding was placed around the parking position to prevent radiation from entering the calorimeter through the collimator aperture. A mini board from Arduino was connected to a nearby computer's USB port to serve as the drive controller [11]. The rail system and driving motor are depicted in Fig. 5.

2.4. Gain monitor system

A light pulser system can be used to calibrate and monitor the gain of a PMT. This approach was found suitable for the SYMB detectors as a means to monitor whether any of the outer crystals' PMTs ever stopped functioning. For this purpose, an LED light source was tested at Mainz University [12] using the mechanical parts shown in Fig. 6. This gain monitoring system was used throughout the OLYMPUS data-taking period.

2.5. Data acquisition electronics

Electronics from the A4 experiment [13] were adapted for the OLYMPUS SYMB readout to allow for fast analog summation of the nine crystals in an array with subsequent digitization and histogramming [14]. The system had an overall dead time of 20 ns, allowing for a histogramming rate of 50 MHz, well above the signal rate.

The signal handling is shown in Fig. 7. First, the nine analog signals (one from each crystal in a sector) are fanned out so that they can be sent to both a sum builder and a "Local Maximum" (LM) veto. The veto accepts an event only if the central crystal in the array had a signal with the highest amplitude, i.e., contained the center of the electromagnetic shower. The sum of all nine signals is split and passed through a constant fraction discriminator (CFD) to three different Analog-to-Digital Converter (ADC) cards, operated in Left Master, Right Master, and Coincidence modes simultaneously. In the first two modes, the named sector is treated as the Master and the opposite sector as the Slave: any signal in the Master detector that passes the Master LM veto and exceeds the CFD threshold is recorded, regardless of what is seen in the Slave sector. In coincidence mode, both sectors are required to have synchronous above-threshold signals and to pass their own LM veto. In this way the LM veto and CFD threshold provide conditions for a trigger,

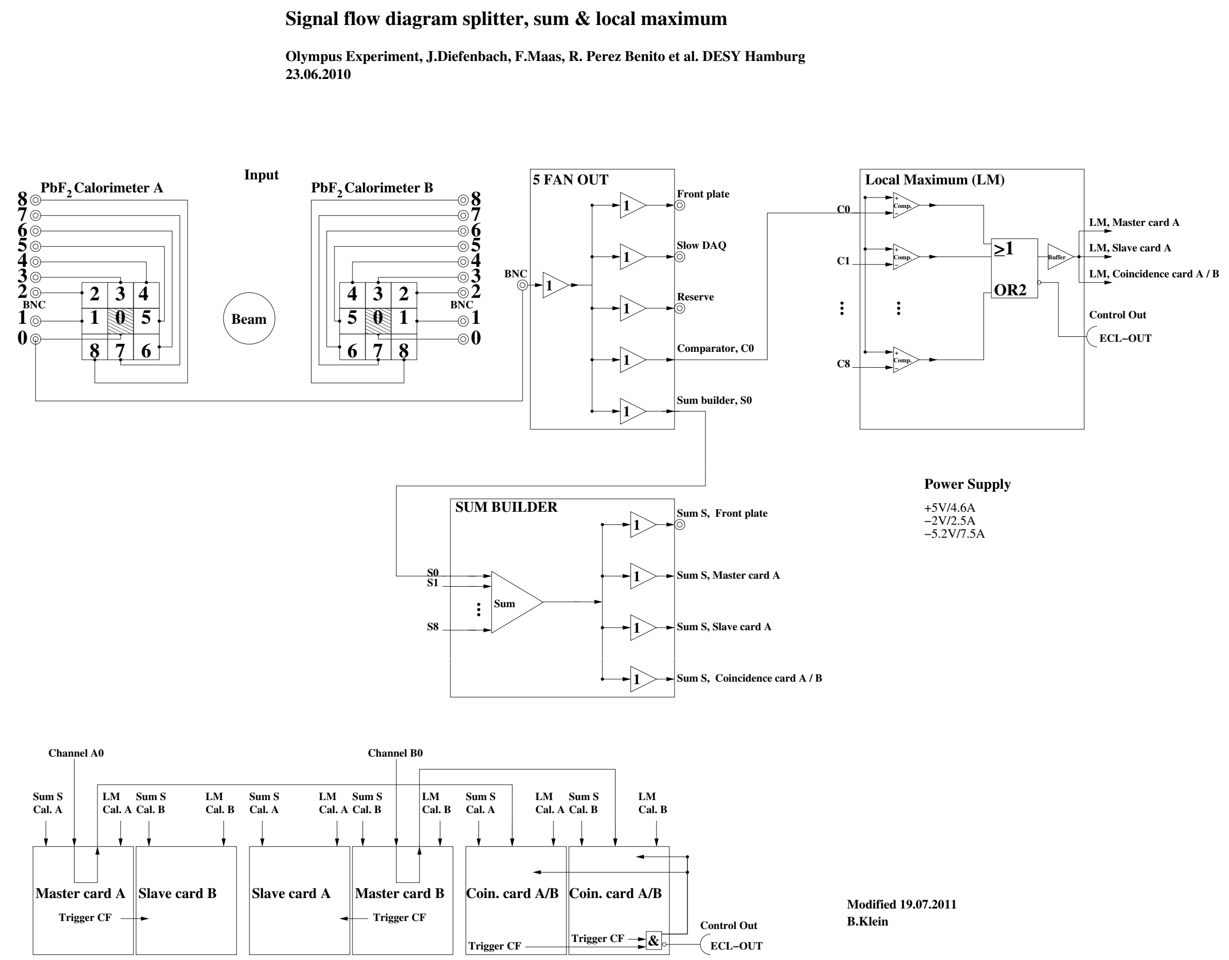

Fig. 7: Schematic for the signal flow in the SYMB data acquisition electronics.

which sends the signals to the histogramming cards for the appropriate mode or modes.

3. Calibration

3.1. PMT gains

All PMTs used needed to be calibrated so that a given amount of light would yield the same signal in each of them. Final gain calibrations were carried out after the PMTs had been glued to the crystals. The high voltage (HV) of the central crystal in each array was used as a reference, while those of the outer crystals were adjusted to produce the same effective gain as was seen in the central crystal. Using a 2 GeV positron beam at Test Area 22 at DESY, a series of measurements was taken at different HVs for each of the outer crystals. A Gaussian filter was applied to the resulting histograms and its first derivative was used to find peak positions. Fig. 8 shows HV versus ADC signal values for a particular outer crystal together with a linear fit. Using these fits, HV values were selected for each crystal to match the gain of the central one. Since the PMTs were never detached from the crystals, it was assumed that the initial calibration would remain valid over the full OLYMPUS data-taking period.

3.2. Energy calibration and resolution

Further calibration was required to ensure that the two SYMB calorimeters would provide the same total signal in response to a lepton beam of the same energy. Using the HV settings from Sec. 3.1, each detector in turn was placed so that the test beam was coaxial with the central crystal while the beam

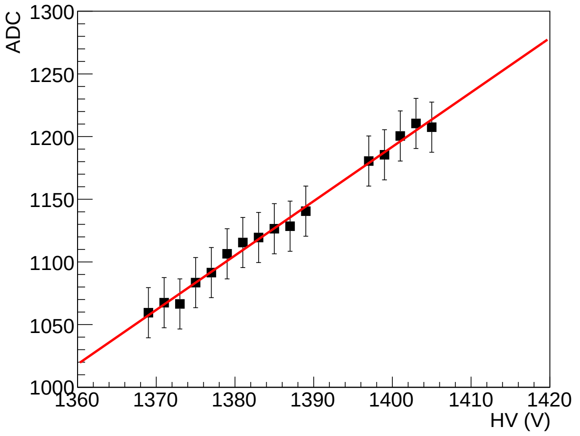

Fig. 8: HV versus ADC channels (black squares) for crystal #4 in the right sector, and a linear fit (red line).

energy was varied in the range of 1 to 2 GeV in steps of 0.2 GeV.

Fig. 9 shows a typical ADC spectrum from the left-sector detector for a 1 GeV electron beam, together with a Gaussian fit. Using the results of the fit to each spectrum, a relationship between the ADC signal and the beam energy was determined. Fig. 10 shows the results for both SYMB detectors, together with individual linear fits for electron and positron beams.

The next step was to determine the energy resolution. The fit to the data points can be parameterized in the following way [15, 16]:

$$\frac{\Delta E}{E} = \sqrt{\left(\frac{a}{E}\right)^2 + \left(\frac{b}{\sqrt{E}}\right)^2 + c^2 + d^2} \qquad (1)$$

where a represents the electronic noise, b is the statistical fluctuations in the number of detected photons, c parameterizes the electromagnetic shower fluctuations on the side boundaries of the crystal arrays, and d is the energy spread of the beam. The energy spread was constant at 3.2% during the test beam, so the given value of d was plugged into the fit function. Fig. 11 shows the measured energy resolution $\Delta E/E$ of each calorimeter for both electron and positron beams. A fit was applied to the data points to extract parameters a, b, and c. Table 1 summarizes the fit results. Shower fluctuations contributed the most to the overall uncertainty in each configuration.

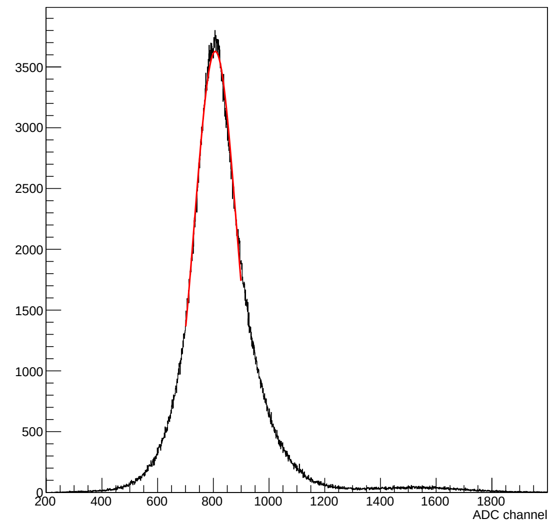

Fig. 9: Typical ADC spectrum (black) fitted with a Gaussian function (red).

4. Operation, Performance, and Results

After calibration, the SYMB detectors were moved into the DORIS beam line together with the whole OLYMPUS apparatus and HV values were set according to the calibration results for optimal detection of SYMB coincidence events.

Fig. 12a is a typical histogram of the SYMB signal in Coincidence mode. ADC values are plotted for the left sector versus the right sector. A broad peak which appears as a red oval in the upper right corner represents the coincidence events in which each primary lepton travels directly through a collimator's aperture and deposits most of its energy in the crystals. Horizontal and vertical bands appear due to one particle partially showering through a collimator brick before reaching the crystals while there is a direct hit in the opposite sector associated with the same scattering event. The bending of these bands toward the edges of the plot can be explained by the fact that the signal pulse is cut by the discriminator's time gate, consequently decreasing the output signal. The positions of the bands and of the oval depend not only on the gain of the ADC card, but also on physical observables such as the position of the lepton beam.

Fig. 12b shows a typical SYMB signal in Master/Slave mode. In addition to the coincidence events (now in the left bottom quarter of the figure due to a roughly factor-of-two difference in gain

Parameter	Left Sector, e^+	Left Sector, e^-	Right Sector, e^+	Right Sector, e^-
a	0.071 ± 0.029	0.073 ± 0.028	0.068 ± 0.007	0.072 ± 0.029
b	0.056 ± 0.051	0.050 ± 0.057	0.070 ± 0.005	0.056 ± 0.053
c	0.029 ± 0.034	0.033 ± 0.029	0.000 ± 0.066	0.030 ± 0.034

Table 1: Summary of the energy resolution fit results for each SYMB detector and each test beam species.

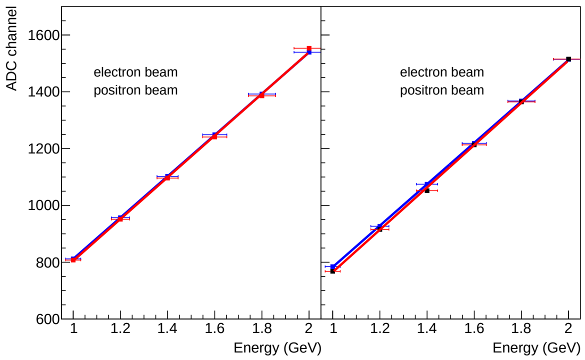

Fig. 10: Energy calibration for the left and right detectors at various beam energies (squares) and fits (lines).

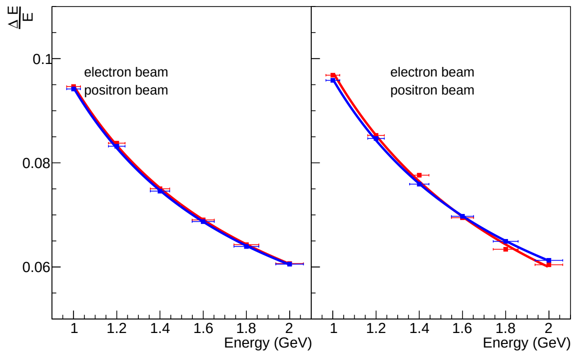

Fig. 11: Energy resolution of the left and right detectors at various beam energies (squares) and fits (lines).

between modes), elastic lepton-proton scattering products can be faintly seen as secondary grid lines along the top and right edges of the data. At their bases, these lines end in more easily visible light-blue peaks.

In SYMB scattering, each product will be roughly 1 GeV but, for a lepton-proton scattering to produce a particle at 1.29°, that particle would be close to 2 GeV. In Fig. 12b, the eye can distinguish two horizontal and two vertical lines, corresponding roughly to these values of energy deposited in either sector. One can imagine a square formed where these lines intersect: the bottom-left corner of the square is brightly visible as the SYMB coincidence peak, but the other corners are not completely vacant, as these are populated by random coincidences between particles produced at different scattering vertices that arrive at the two calorimeters simultaneously.

There is a visible effect in Figs. 12a and 12b due to differential nonlinearities in the ADC cards. The ADC bin widths, in energy, are not all identical, but each bin represents one bit in the digitized output. Therefore, occasional thin lines (of width one bin) may appear horizontally or vertically that contain slightly more or fewer counts than the surrounding bins. This is a minor effect, handled in the detailed analysis, but it can give the images the appearance of an aliasing error.

During the first OLYMPUS run in early 2012, measurements from the SYMB calorimeters and other luminosity monitors revealed an observed luminosity that was roughly one-eighth of the expected value. That allowed for the identification of a significant hydrogen leak in the target, which was then repaired. Luminosity measurements subsequently confirmed an increase up to nominal levels.

Fig. 13 demonstrates agreement between two independent subsystems designed to determine the luminosity at OLYMPUS. The SYMB detectors count coincidences to enable a comparison between the number of roughly symmetric SYMB events within the acceptance region when running with an electron beam and that when running with a positron beam. Counts are integrated over discrete readout periods, whose durations are determined by the rate of lepton-proton scatters counted by the OLYMPUS spectrometer, but which typically last about half a minute. Plotting the number of SYMB events counted in one readout period versus the integrated luminosity in that same time, as determined by the slow control, one sees two linear relationships: the upper line corresponds to an elec-

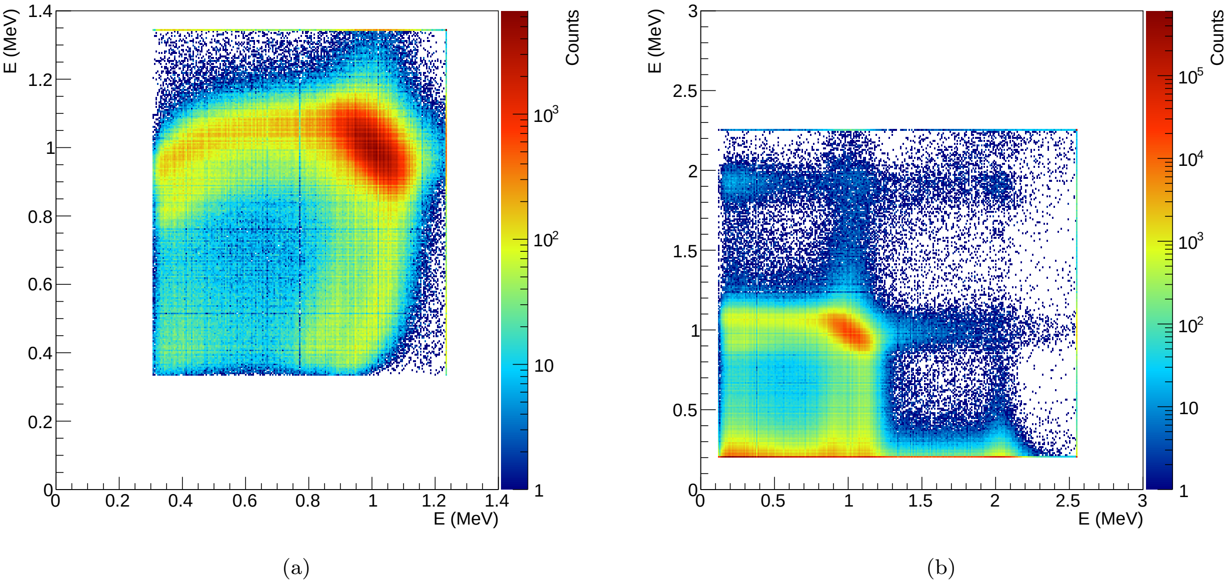

Fig. 12: Typical signal of the SYMB in the coincidence mode (a) and right-master left-slave mode (b).

tron beam and the line with a shallower slope corresponds to a positron beam, since the acceptance-integrated cross section is higher for Møller events than for Bhabha scatters and pair annihilation.

The data in Fig. 13 covers the last two months of data collection. There is some width to the lines, and a few readout periods are separated from the main pattern. However, since this comparison relates two independent measurements of the same observable, it is encouraging that they bear a clear linear relationship. This is the sort of relationship one would expect from distinct luminosity measurements if each of the two approaches yielded accurate results.

Between the first and second data runs, HVs were reset to nominal values and four 6 dB attenuators were installed for use in the Master/Slave modes. This effectively doubled the dynamic range of the histogramming cards and successfully allowed for the detection of elastic lepton-proton scattering products throughout the remainder of data taking.

During the second run in late 2012, several beam position and beam slope scans were performed as tests. In each scan, the DORIS beam's position or slope at the target center was varied along either the vertical or the horizontal axis while remaining fixed along the other axis. Fig. 14 shows normalized count rates for four scans of beam position along the horizontal axis. These tests demonstrated the sensitivity of the SYMB detectors to beam movements and enabled the optimization of the beam position to maximize SYMB rates.

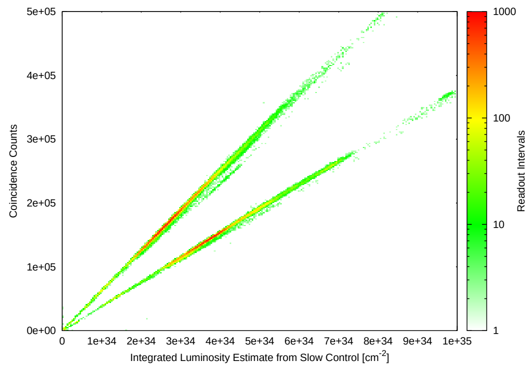

Fig. 13: SYMB counts scale linearly with the luminosity estimate from an independent subsystem.

5. Simulation

Detailed Monte Carlo studies have been carried out to aid in characterization of the signal, understanding of systematics, and calibration of analysis

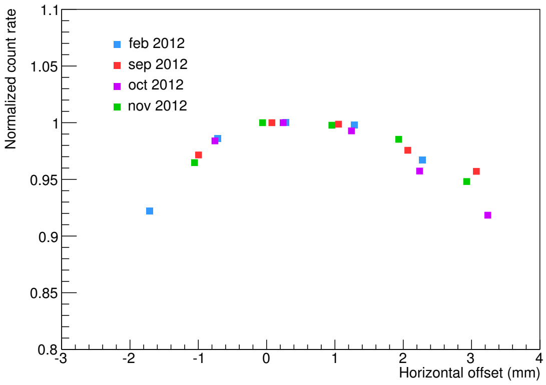

Fig. 14: Normalized count rate in the SYMB during several beam scans performed throughout the data taking.

parameters such as cut placements. These studies utilized the OLYMPUS simulation framework, which is divided into three sequential steps: event generation, particle propagation, and digitization.

5.1. Event generation and propagation

Simple event generators that produce final states (i.e., pairs of particles) for Møller scattering, Bhabha scattering, and pair annihilation have been written using tree level cross section formulas. A more advanced set of generators, including next-to-leading order radiative corrections, is being developed and is intended for use in the full OLYMPUS analysis (C. Epstein, in preparation). Based on the input beam species and energy, a kinematically allowed result is selected randomly according to a sampling distribution that approximates the cross section as a function of the scattering angle. The generator assigns the appropriate four-momentum to each outgoing lepton or photon, and their initial position at the event vertex is determined based on the spatial density distribution of the simulated gaseous hydrogen target cell and beam position information that can be artificial or derived from monitor readings in the OLYMPUS data stream. Each event also receives a numerical weight at generation time, accounting for the sampling distribution as well as the physical cross section of the event's final state, which is used in the final analysis to ensure proper statistics.

Generated particles are propagated through a realistic solid model of the OLYMPUS apparatus based on GEANT4 [17]. Detector placements, based on *in situ* surveys, are maintained in the GDML file format [18]. Typically, a primary particle will fly down the beam pipe, bending incrementally in the magnetic field, until it passes through the collimator and impinges on the calorimeter, beginning an electromagnetic shower. Every secondary particle in the cascade is tracked by GEANT4 so that the distribution of energy deposits from ionization are as accurate as possible, with realistic variance. The energy deposit in each crystal, such as in Fig. 15a, is the output of the propagation step.

5.2. Digitization

Simulated events are intended to be analyzed in exactly the same way as observed events. This requires a digitization step, in which data, formatted identically to the output of the detector is obtained from the energy deposition produced by GEANT4.

Since PbF_2 is a pure Cherenkov calorimeter, it would be ideal to use the optical methods of GEANT4 to have every charged particle in the showers generate cones of light and to use ray tracing to follow the photons until they either register in a photomultiplier tube (PMT) or are lost. A less computationally expensive approach has been derived from [19]. First, for each instance of energy loss in GEANT4, an estimate is obtained for the number of photoelectrons produced in the PMT due to Cherenkov light from the charged particle whose energy was lost since its last such loss (Fig. 15b). This estimate makes use of a parametrization based on data obtained using PbF_2 crystals like those in the detector.

Second, a digital ADC signal is determined as a linear function of the number of photoelectrons in the PMT. The coefficient and scalar offset were obtained from calibration data. Fig. 15c shows ADC signals from Monte Carlo simulation for both the left and right detector modules.

The digitization process accounts for systematic effects and statistical fluctuations due to the associated electronics used in the experiment. Finally, artificial ADC signals from simulation are recorded in ROOT [20] trees with the same structure as the raw OLYMPUS data so that both can be analyzed in the same way.

Because of subtle effects from the data acquisition electronics that manifest in the raw SYMB data, it isn't possible for the simulated results to perfectly match the empirical results. However, an accurate simulation allows for signal and noise to be

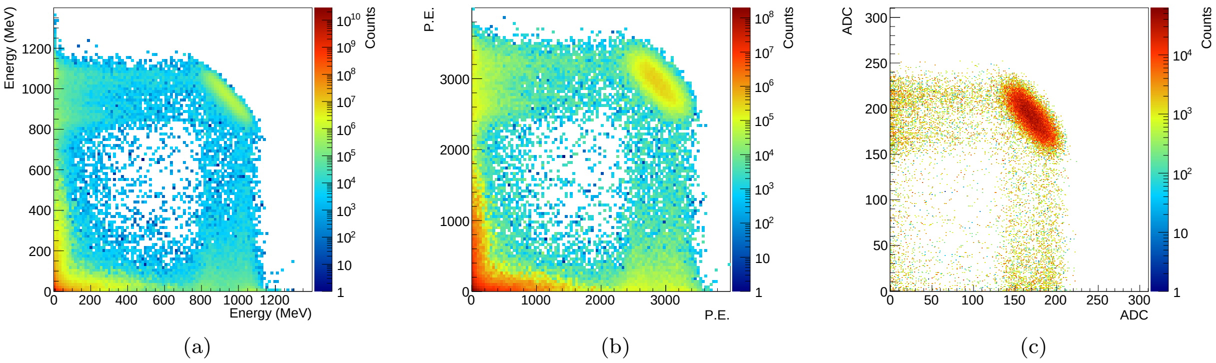

Fig. 15: SYMB digitization process, left sector versus right: (a) energy deposition, (b) number of photoelectrons produced, and (c) ADC signal for Møller scattering.

distinguished in the data by comparison to a noise-free result from Monte Carlo, and using the same approach to simulate both the electron beam and the positron beam aids in identifying any charge-asymmetric effects in the analysis. In order to produce a precise relative luminosity measurement, it is crucial to prevent significant systematic effects from data selection techniques that treat Møller events and Bhabha events on unequal footing.

6. Conclusion

The design of a luminosity monitoring system, consisting of a pair of Cherenkov electromagnetic calorimeters, has been presented along with a detailed explanation of their use as luminosity monitors in the OLYMPUS experiment. From the data obtained using these detectors, integrated rates of lepton-lepton scattering events are being determined now as a function of time over the full running period. Such empirical results can be compared to theoretical expectations by means of a full simulation that accounts for beam dynamics, first-order and radiative scattering processes, and the geometry of the apparatus. Relative luminosity values can thus be obtained with tightly constrained systematic variance and high statistics, providing an adequate normalization for the OLYMPUS experiment's precision measurement of the electron-proton to positron-proton elastic scattering cross section ratio.

7. Acknowledgments

This work is indebted to the A4 collaboration for their thorough studies of lead fluoride crystals as Cherenkov calorimeters. We are thankful to the electronics workshop from IKPH Mainz, particularly Mr. Klein and Dr. Lauth for discussing the A4 electronics with us at length; as well as the mechanical workshop from IKPH Mainz, especially Mr. Luzius. We gratefully acknowledge Dr. Yang for performing simulations of mu-metal boxes. The authors also wish to thank all our collaborators in the OLYMPUS experiment and the staff at DESY, where not only the data collection but most of the calibration of the detectors took place.

This work was supported by the Office of Nuclear Physics of the U.S. Department of Energy, Grant no. DE-FG02-94ER40818.

References

[1] P. A. Guichon, M. Vanderhaeghen, How to reconcile the Rosenbluth and the polarization transfer method in the measurement of the proton form-factors, Physical Review Letters 91 (2003) 142303. arXiv:hep-ph/0306007, doi:10.1103/PhysRevLett.91.142303.

[2] J. Arrington, P. Blunden, W. Melnitchouk, Review of two-photon exchange in electron scattering, Progress in Particle and Nuclear Physics 66 (2011) 782. arXiv:1105.0951, doi:10.1016/j.ppnp.2011.07.003.

[3] R. Milner, D. Hasell, M. Kohl, U. Schneekloth, N. Akopov, et al., The OLYMPUS experiment, Nuclear Instruments and Methods in Physics Research Section A 741 (2014) 1–17. arXiv:1312.1730, doi:10.1016/j.nima.2013.12.035.

[4] D. Hasell, T. Akdogan, R. Alarcon, W. Bertozzi, E. Booth, et al., The BLAST experiment, Nuclear Instruments and Methods in Physics Research Section A 603 (2009) 247–262.

[5] Y. Tsai, High-energy electron-electron scattering, Physical Review 120 (1960) 269–286. doi:10.1103/PhysRev.120.269.

[6] S. Baunack, et al., Measurement of strange quark contributions to the vector form factors of the proton at Q^2 = 0.22 (GeV/c)^2, Phys. Rev. Lett. 102 (2009) 151803. doi:10.1103/PhysRevLett.102.151803.

[7] J. Beringer, et al., Review of particle physics, Phys. Rev. D 86 (2012) 010001. doi:10.1103/PhysRevD.86.010001.

[8] P. Achenbach, et al., Measurements and simulations of Cherenkov light in lead fluoride crystals, Nuclear Instruments and Methods in Physics Research Section A: Accelerators, Spectrometers, Detectors and Associated Equipment 465 (23) (2001) 318 – 328. doi:http://dx.doi.org/10.1016/S0168-9002(01)00668-4.

[9] P. Achenbach, et al., Radiation resistance and optical properties of lead fluoride Cherenkov crystals, Nuclear Instruments and Methods in Physics Research Section A: Accelerators, Spectrometers, Detectors and Associated Equipment 416 (23) (1998) 357 – 363. doi:http://dx.doi.org/10.1016/S0168-9002(98)00748-7.

[10] S. Köbis, Entwicklung eines Triggersystems zur Selektion elastischer Elektronenstreuereignisse in einem schnellen Kalorimeter, Ph.D. thesis, Johannes Gutenberg-Universität, Mainz, Germany (1998).

[11] E. Göbel, Bau eines Moller/Bhabha-Luminositätsmonitors für das Olympusexperiment am DESY in Hamburg, Masters thesis, Johannes Gutenberg-Universität, Mainz, Germany (2011).

[12] W. Rehmann, Aufbau eines LED-Lichtpulsersystems fluoride für das OLYMPUS-Experiment, Bachelors thesis, Johannes Gutenberg-Universität, Mainz, Germany (2011).

[13] S. Köbis, et al., The analog trigger processor for the new parity violation experiment at MAMI, Nuclear Physics B - Proceedings Supplements 61 (3) (1998) 625 – 629, proceedings of the Fifth International Conference on Advanced Technology and Particle Physics. doi:http://dx.doi.org/10.1016/S0920-5632(97)00629-4.

[14] R. Kothe, Design and operation of fast calorimeter electronics for an experiment for the measurement of the parity violation in elastic electron scattering, Ph.D. thesis, Johannes Gutenberg-Universität, Mainz, Germany (2008).

[15] V. Berestetskii, E. Lifshitz, L. Pitaevskiĭ, Quantum Electrodynamics, Pergamon Press, 1982.

[16] T. Benisch, The luminosity monitor of the HERMES expeiment at DESY, Ph.D. thesis, Universität Erlangen-Nürnberg (2000).

[17] S. Agostinelli, et al., Geant4—a simulation toolkit, Nuclear Instruments and Methods in Physics Research Section A: Accelerators, Spectrometers, Detectors and Associated Equipment 506 (3) (2003) 250 – 303. doi:http://dx.doi.org/10.1016/S0168-9002(03)01368-8.

[18] R. Chytracek, J. McCormick, W. Pokorski, G. Santin, Geometry description markup language for physics simulation and analysis applications, Nuclear Science, IEEE Transactions on 53 (5) (2006) 2892–2896. doi:10.1109/TNS.2006.881062.

[19] L. Capozza, Untergrundstudien zur Messung der Strangeness-Vektorformfaktoren des Protons durch paritätsverletzende Elektronenstreuung unter Rückwartswinkeln, Ph.D. thesis, Johannes Gutenberg-Universität, Mainz, Germany (2010).

[20] R. Brun, F. Rademakers, ROOT - an object oriented data analysis framework, Nuclear Instruments and Methods in Physics Research Section A: Accelerators, Spectrometers, Detectors and Associated Equipment 389 (12) (1997) 81 – 86, new Computing Techniques in Physics Research V. doi:http://dx.doi.org/10.1016/S0168-9002(97)00048-X.